Geomechanics and Engineering, *Vol. 29, No. 4 (2022) 391-405*
https://doi.org/10.12989/gae.2022.29.4.391

Combined bi-borehole technology for grouting and blocking of flowing water in karst conduits: Numerical investigation and engineering application

Dongdong Pan[1,2], Yichi Zhang[1,3], Zhenhao Xu*[1,3], Haiyan Li[1,2] and Zhaofeng Li[1,2]

[1]*Geotechnical and Structural Engineering Research Center, Shandong University, Jinan, Shandong 250-061, China*
[2]*School of Civil Engineering, Shandong University, Jinan, Shandong 250-061, China*
[3]*School of Qilu Transportation, Shandong University, Jinan, Shandong 250-061, China*

(Received February 3, 2021, Revised March 2, 2022, Accepted March 4, 2022)

Abstract. A newly proposed grouting simulation method, the sequential diffusion solidification method was introduced into the numerical simulation of combined bi-borehole grouting. The traditional, critical and difficult numerical problem for the temporal and spatial variation simulation of the slurry is solved. Thus, numerical simulation of grouting and blocking of flowing water in karst conduits is realized and the mechanism understanding of the combined bi-borehole technology is promoted. The sensitivity analysis of the influence factors of combined bi-borehole grouting was investigated. Through orthogonal experiment, the influences of proximal and distal slurry properties, the initial flow velocity of the conduit and the proximal and distal slurry injection rate on the blocking efficiency are compared. The velocity variation, pressure variation and slurry deposition phenomenon were monitored, and the flow field characteristics and slurry outflow behavior were analyzed. The interaction mechanism between the proximal and distal slurries in the combined bi-borehole grouting is revealed. The results show that, under the orthogonal experiment conditions, the slurry injection rate has the greatest impact on blocking. With a constant slurry injection rate, the blocking efficiency can be increased by more than 30% when using slurry with weak time-dependent viscosity behavior in the distal borehole and slurry with strong time-dependent viscosity behavior in the proximal borehole respectively. According to the results of numerical simulation, the grouting scheme of "intercept the flow from the proximal borehole by quick-setting slurry, and grout cement slurry from the distal borehole" is put forward and successfully applied to the water inflow treatment project of China Resources Cement (Pingnan) Limestone Mine.

Keywords: blocking mechanism; combined bi-borehole grouting; flowing water grouting; orthogonal experiment

1. Introduction

Karst water inflow hazard is a serious threat to the safety of underground engineering construction (Andjelkovic 2013, Stille *et al*. 2012, Xu *et al*. 2021a, Xu *et al*. 2021b). Grouting is one of the main means to deal with water inflow hazard (Kim and Moon 2020, Minto *et al.* 2016). The researches on grouting theory applied to pores and fractures are earlier and more fully developed (Ghafar *et al*. 2016, Mu *et al*. 2019). In engineering practice, the water inflow quantity in fractures is mild and the flow velocity is limited, the blocking difficulty is less severe (Draganović and Stille 2014, El Tani 2012, Xu *et al*. 2021c). For conduit grouting, the high velocity groundwater in karst conduits and the large cavity volume are not conducive to the deposition and solidification of slurry (Mohammed *et al.* 2014). The grouting process lasts for a long time with serious slurry outflow, which puts forward higher requirements for grouting technology. The combined bi-borehole grouting technology improves the slurry retention rate, and it is suitable to block flow water in karst conduits (Li 2018). However, due to the limitations of existing experimental and numerical simulation methods, the understanding of its mechanism is limited to the summary of engineering experience, and no systematic explanation has been given.

It is difficult to study the blocking mechanism of conduit grouting by means of experimental methods (Gustafson *et al.* 2013, Sharpe 1990). Taking model experiment as an example, most experiments on blocking mechanism are summaries of slurry flow in fractures (Aflaki and Moodi 2017, Sui *et al*. 2015, Yang *et al*. 2020, Zou *et al*. 2018). In contrast, conduit grouting experiment is difficult to carry out and the data acquisition is not ideal due to the solidification of the slurry as the slurry is easy to block the conduits, thus affecting normal operation of sensors and damaging experimental system.

Therefore, the study of blocking mechanism by numerical simulation has become an important analysis method of conduit grouting. In computational fluid dynamics, the blocking of karst conduits by grouting is a complex two-phase system. Compared with fracture grouting, perspectives such as treats slurry viscosity as a constant or a power function and displacement flow are no longer accurate (Funehag and Thörn 2018). The viscosity of slurries used in grouting, such as cement slurry and cement-based quick-setting slurry, has obvious spatiotemporal evolution behavior (Rahman *et al*. 2015). Scholars have

*Corresponding author, Professor
E-mail: zhenhao_xu@sdu.edu.cn

ISSN: 2005-307X (Print), 2092-6219 (Online)

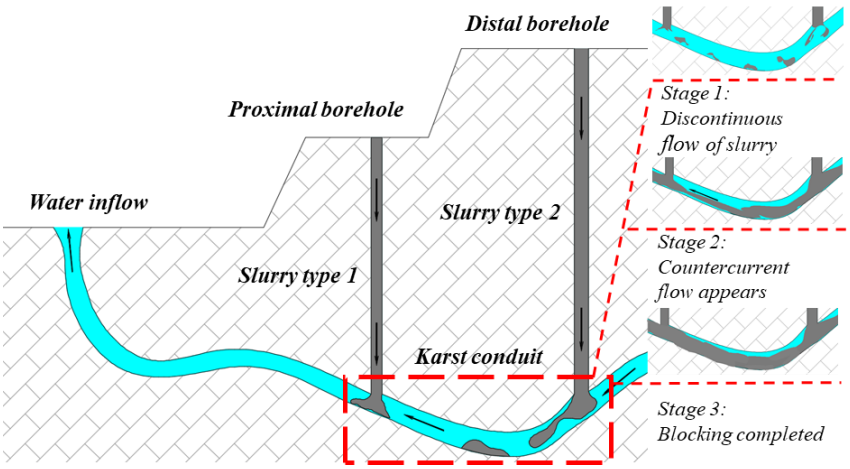

Fig. 1 Specific implementation of combined bi-borehole grouting

measured the slurry viscosity variation behavior and regarded slurry as Bingham fluid (Amadei and Savage 2001, Gullu 2017, Li *et al*. 2013). This is quite different from the sediment formation in pipelines for numerical simulations in other fields (Chi *et al*. 2019, Ismail *et al*. 2015, Magnini and Matar 2019). In the existing methods, the assumption that the slurry viscosity is a constant or power function is acceptable in fracture grouting (Hao *et al*. 2018, Nadimi and Shahriar 2014, Puay and Hosoda 2016). However, due to the longer time span, the viscosity and slurry flow range when conducting conduit grouting are greatly different from the actual situation, and the calculation is easy to diverge. Therefore, the existing grouting simulation methods cannot be effectively applied to the numerical simulation of conduit grouting. In recent years, although scholars have developed some improved methods, there is still a lack of numerical methods to accurately describe the slurry viscosity variation behavior (Ao *et al*. 2017, Ghareh *et al.* 2020, Huang *et al.* 2020, Lee *et al*. 2016, Liu *et al*. 2020, Mohajerani *et al*. 2015). In order to solve the above problems, we proposed a sequential diffusion solidification (SDS) method considering the temporal and spatial evolution of slurry viscosity. Compared with traditional methods, it successfully solved the numerical problem of slurry viscosity variation, and provided a reliable numerical method for conduit grouting simulation (Li *et al*. 2020, Xu *et al.* 2021d, Xu *et al.* 2022).

In this study, based on the fluid volume method, the numerical simulation of combined bi-borehole flowing water grouting in the karst conduit was studied by finite volume discretization. In the slurry viscosity model, the SDS method which is more accurate in describing the time-dependent viscosity behaviors of slurry is used. In addition, the variation of velocity and pressure in the karst conduit and the behavior of slurry flow and deposition are analyzed. The blocking mechanism of karst conduit grouting is explored. Based on the above content, we design a 5-factor mixed level orthogonal experiment, and optimize the parameters of combined bi-borehole grouting according to the orthogonal experiment results. Finally, it was successfully applied to the water inflow treatment project of China Resources Cement (Pingnan) Limestone Mine.

2. Combined bi-borehole technology for flowing grouting and blocking of flowing water

In engineering practice, due to the performance of grouting equipment, the flow capacity of slurry and the connectivity between the boreholes and the water passage, karst conduits and wide fractures with high flow velocity cannot be blocked only through single borehole grouting. In contrast, combined bi-borehole grouting can effectively improve the blocking efficiency. As shown in Fig. 1, the specific implementation method is to grout two boreholes simultaneously, which have good connectivity with the karst conduit, so as to reduce water flow and increase slurry retention.

Generally speaking, the boreholes can be divided into proximal borehole and distal borehole according to the distance from water inflow point. Different grouting parameters, including slurry type and slurry injection rate are often selected for proximal and distal boreholes. However, the interaction between the proximal and distal slurries is not considered in traditional grouting theories. Currently there is no corresponding theoretical support, and the understanding of blocking mechanism only stays on summaries of engineering experiences.

In this paper, numerical simulation is carried out based on the SDS method, and the blocking mechanism of combined bi-borehole grouting and the optimization of grouting parameters of proximal and distal boreholes are studied by orthogonal experiment. The grouting scheme of "intercept the flow from the proximal borehole by quick-setting slurries and grout cement slurries from the distal borehole" is put forward and successfully applied to the water inflow treatment project of China Resources Cement (Pingnan) Limestone Mine.

3. Numerical Investigation

3.1 Sequential diffusion and solidification (SDS) method

Considering the requirements of capturing the phase

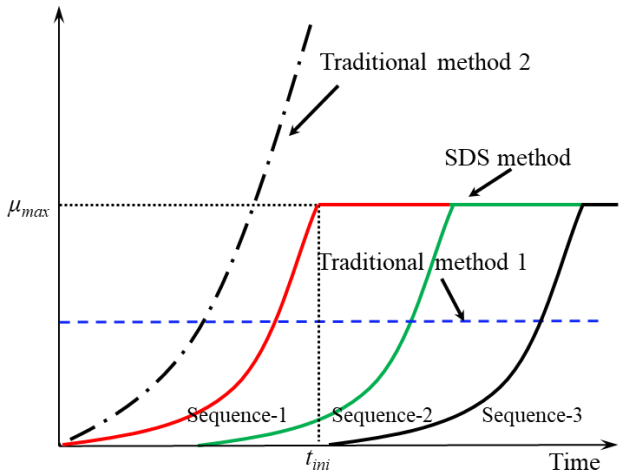

Fig. 2 Viscosity variation of slurry in traditional methods and the SDS method

interface and simulating on the engineering scale, the volume of fluid method and the Reynolds stress turbulence model have better simulation performance (Kaushal *et al.* 2012, Wang *et al.* 2020, Zou *et al.* 2017). The governing equations of the SDS method are basically consistent with the volume of fluid method, including continuity equation, momentum equation and phase fraction equation

$$\nabla \cdot U = 0 \tag{1}$$

$$\frac{\partial \rho U}{\partial t} + \nabla \cdot \left(\rho U U \right) = \nabla \cdot \tau + S \tag{2}$$

$$\frac{\partial \alpha}{\partial t} + \nabla \cdot \left(\rho U \alpha \right) = 0 \tag{3}$$

where U is the velocity vector of fluid, ρ is the density of fluid, t is the time, τ is the Shear stress, S is the source term, α is the phase volume fraction. The value of phase volume fraction of slurry can be expressed as

$$\alpha = \begin{cases} 0 & \textit{within water phase} \\ 0 < \alpha < 1 & \textit{within interface region} \\ 1 & \textit{within slurry phase} \end{cases} \tag{4}$$

As shown in Fig. 2, it is different from the traditional method which regards the slurry viscosity as a constant or continuously growing power function, the SDS method describes slurry flow in sequence according to its time-dependent viscosity behaviors. From the beginning of grouting, the next sequence of slurry is injected after a fixed time span Δt. The slurries of different sequences obey their independent viscosity variation functions. The term "sequential" used here actually represents the time sequence of the slurry that was injected into karst mediums. After the *j*-th sequential slurry started to be injected, the viscosity μ_i at time t can be expressed as

$$\mu_i = \begin{cases} A\left[t - (i-1)\Delta t \right]^n + \mu_{\min} & (i-1)\Delta t < t < t_{ini} \\ \mu_{\max} & t \geq t_{ini} \end{cases} \tag{5}$$

where *A, n* are the coefficients determined according to different types of slurries.

The viscosity variation of each sequential slurry can be divided into the growth stage and the solidification stage. In the growth stage, the variation of slurry viscosity follows the power function. For a certain sequential slurry passing through t_{ini} period, the viscosity increases to the threshold $\mu_{\max}$, which indicates that this sequential slurry has reached the solidification stage, and its viscosity remains constant. Compared with the traditional method that the slurry viscosity increases infinitely or is regarded as a constant, this method is closer to real situation.

Meanwhile, the increase of slurry sequences means the increase of equation quantity. According to the characteristics of large temporal and spatial span of the calculation domain in this study, it is necessary to correct the slurry whose viscosity reaches the threshold. The specific process is as follows.

When Δt is the sequence interval, volume fraction of the first sequence is taken as the basis. The flow region where the viscosity of slurry reaches $\mu_{\max}$ is obtained from calculation region, which is recorded as $\Omega_{\mu\max}$. The flow time of the *j*-th sequential slurry reaches the viscosity threshold value is recorded as t_j. The time of different sequential slurries that reach the solidification stage can be expressed as

$$t_j = t_{ini} + j \cdot \Delta t (j = 1,2,\ldots,n-1) \tag{6}$$

At t_j moment, the *j*-th sequential slurry was corrected. The regions occupied by water and different sequential slurries can be expressed as $\Omega_w^{j-1}, \Omega_{s1}^{j-1}, \Omega_{s2}^{j-1}, \ldots, \Omega_{sn}^{j-1}$, respectively. The following is the correction method of the *j*-th sequential slurry

$$\Omega_{s1}^{j} = \Omega_{s1}^{j-1} + \Omega_{s2}^{j-1}, \Omega_{s2}^{j} = \Omega_{s3}^{j-1}, \ldots, \Omega_{s(n-1)}^{j} = \Omega_{sn}^{j-1} \left(1 \leq j \leq n \right) \tag{7}$$

The physical model of different sequential slurries is reconstructed by correction, and their viscosities are corrected as follows

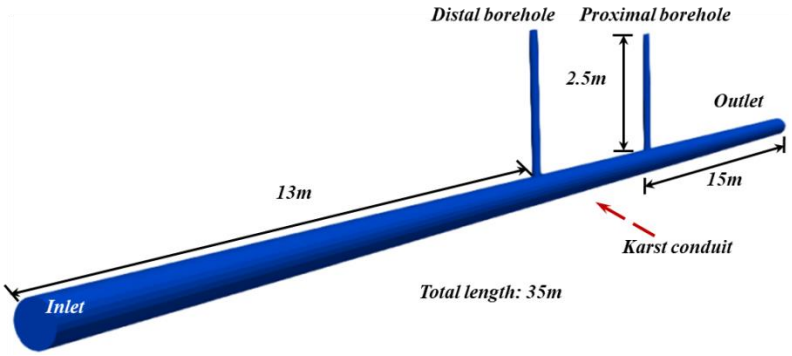

Fig. 3 Model of combined bi-borehole grouting

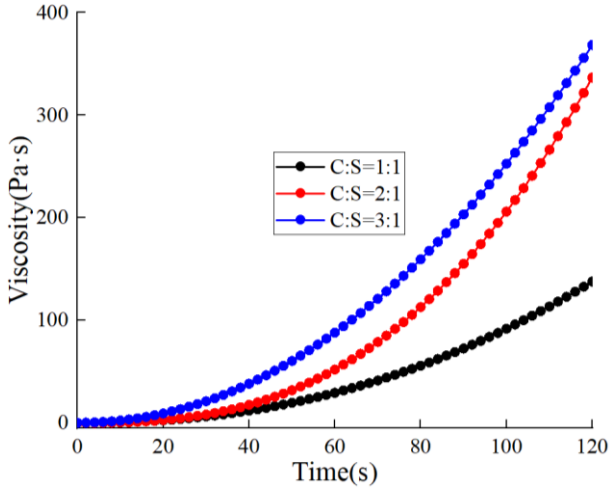

Fig. 4 Time-dependent function of slurry viscosity

$$\mu_{S_{An}}^{j}(t) \leftarrow \mu_{S_{An}}^{j-1}(t) = A\left[t-(j+A_n)\Delta t\right]^n + \mu_{\min}\left(\Omega^j \cap \Omega_{S_{An}}^{j}\right) \cap \left(t_{ini}+j\Delta t < t < t_{ini}+(j+1)\Delta t\right) \quad (8)$$

where $\mu_{S_n}^{j}$ is the corrected viscosity. S_n denotes different sequential slurries, $A = f\left\lfloor \frac{t_{ini}}{\Delta t} \right\rfloor$.

The SDS method describes behavior of the slurry viscosity in a relatively real way as time and space change. The feasibility of the SDS method in numerical simulation has been verified (Li *et al*. 2020).

3.2 Computational model and experimental design

In order to study the blocking mechanism of combined bi-borehole grouting technology, the SDS method was used to study the blocking process in numerical simulation. The conclusion can be extended to the process optimization of combined multi-borehole grouting technology.

As shown in Fig. 3. The karst conduit is regarded as a smooth conduit. The karst conduit model is 35 m long and 0.5 m in diameter. According to the distance to the outlet of the karst conduit, it can be divided into distal grouting borehole and proximal grouting borehole. The position of the distal and proximal grouting borehole is 13 m and 20 m away from the inlet of the karst conduit, respectively. The depth of each borehole is 2.5 m and the diameter is 0.15 m. Boreholes intersect with the karst conduit vertically.

The profile of the karst conduit is determined according to the practice of water inflow treatment project of China Resources Cement (Pingnan) Limestone. In this project, boreholes were spaced about 5.4 ~ 8.7 m in a grout curtain, so the distance between the proximal and distal boreholes is determined to be 7 m in our numerical simulation. According to the karst conduit revealed by drilling, the average height of the conduit is 0.507 m, so we define 0.5 m as the diameter of the karst conduit model. Besides, in this project, the diffusion radius of the slurry is assumed to be 6 m. Thus, the total length of the karst conduit model should be larger than 19 m. In order to expand the computational domain as much as possible, the length of the karst conduit model is set at 35 m.

As shown in Table 1, this study selects initial water flow velocity, distal and proximal slurry properties, distal and proximal slurry injection rate as influence factors in the study of karst conduit flowing water blocking mechanism. The 5 factors mixing level orthogonal experiment was designed. It should be noted that the slurry properties in the numerical simulation are determined according to the quick-setting slurry composed of cement and sodium silicate. Its viscosity increased according to the time-dependent function measured by scholars (Li *et al*. 2013).

Table 1 Calculation parameters in orthogonal experiment

Level	Initial flow velocity (m/s)	Distal slurry properties (C:S)	Proximal slurry properties (C:S)	Distal slurry injection rate (m/s)	Proximal slurry injection rate (m/s)
1	0.8	1:1	1:1	0.2	0.2
2	0.6	2:1	2:1	0.35	0.35
3		3:1	3:1	0.5	0.5

Table 2 Parameters setting of each case in orthogonal experiment

Case number	Initial flow velocity (m/s)	Distal slurry properties (C:S)	Proximal slurry properties (C:S)	Distal slurry injection rate (m/s)	Proximal slurry injection rate (m/s)
Case1	0.8	1:1	1:1	0.2	0.2
Case2	0.8	1:1	2:1	0.35	0.35
Case3	0.8	1:1	3:1	0.5	0.5
Case4	0.8	2:1	1:1	0.2	0.35
Case5	0.8	2:1	2:1	0.35	0.5
Case6	0.8	2:1	3:1	0.5	0.2
Case7	0.8	3:1	1:1	0.35	0.2
Case8	0.8	3:1	2:1	0.5	0.35
Case9	0.8	3:1	3:1	0.2	0.5
Case10	0.6	1:1	1:1	0.5	0.5
Case11	0.6	1:1	2:1	0.2	0.2
Case12	0.6	1:1	3:1	0.35	0.35
Case13	0.6	2:1	1:1	0.35	0.5
Case14	0.6	2:1	2:1	0.5	0.2
Case15	0.6	2:1	3:1	0.2	0.35
Case16	0.6	3:1	1:1	0.5	0.35
Case17	0.6	3:1	2:1	0.2	0.5
Case18	0.6	3:1	3:1	0.35	0.2

For convenience, we also list it in Fig. 4, where C:S refers to the volume ratio of cement to sodium silicate. The C:S=1:1 slurry has the weakest time-dependent viscosity behavior, and the C:S=3:1 slurry has the strongest time-dependent viscosity behavior. The specific case settings are shown in Table 2.

3.3 Flow and deposition process of combined bi-borehole grouting

3.3.1 Flow rate variation of flowing water in combined bi-borehole grouting

As shown in Fig. 5, typical cases are selected to analyze the variation of flow rate in combined bi-borehole grouting. The results show that the decrease rate in case3 and case9 is greater than in other cases. When the grouting lasted for 40 s, the flow rate in case3 and case9 decreased to 0.092 m3/s and 0.087m3/s, respectively. It can be seen that the proximal grouting injection rate of 0.5 m/s is the main influence factor. On the contrary, although case10 and case11 have low initial flow velocity, case10 uses slurry of

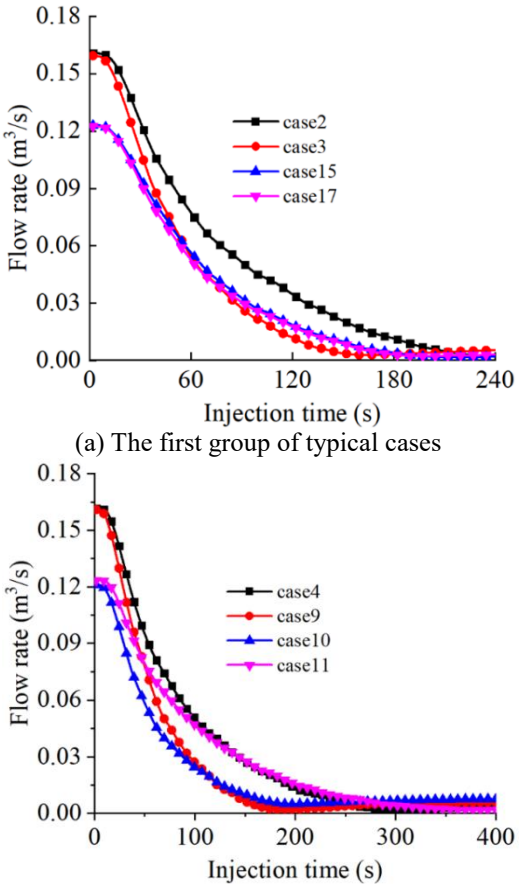

(a) The first group of typical cases

(b) The second group of typical cases

Fig. 5 Variation curve of the flow rate at the outlet of conduit

C:S=1:1 in both the proximal and distal boreholes, which leads to a slow solidification process. Case11 uses the minimum slurry injection rate, as a result, it is difficult to reduce the flow rate in karst conduit in time. Because case9 uses slurry of C:S=3:1 and a high slurry injection rate at the proximal borehole, the blocking time was reduced by 49.7% compared with case11. Case3 ensures its blocking efficiency by selecting slurry of C:S=3:1 at the proximal borehole and slurry of C:S=1:1 at the distal borehole and increasing slurry injection rate.

3.3.2 Pressure variation in combined bi-borehole grouting

As shown in Fig. 6(a), typical cases for the pressure variation at the bottom of distal borehole are selected for analysis. In the process of blocking, the variation of grouting pressure can be divided into three stages. In the first stage, there is no stable slurry deposition at the bottom of the conduit, and the pressure increases slowly. Take case16 as an example, the first stage was from 0 s to 45 s.

In the second stage, the slurry at the bottom of the boreholes began to deposit stably, and the pressure growth rate was higher than that in the first stage. Taking case8 as an example, the second stage was from 60 s to 165 s, which lasted until the completion of blocking. The third stage starts from the completion of blocking, and the pressure

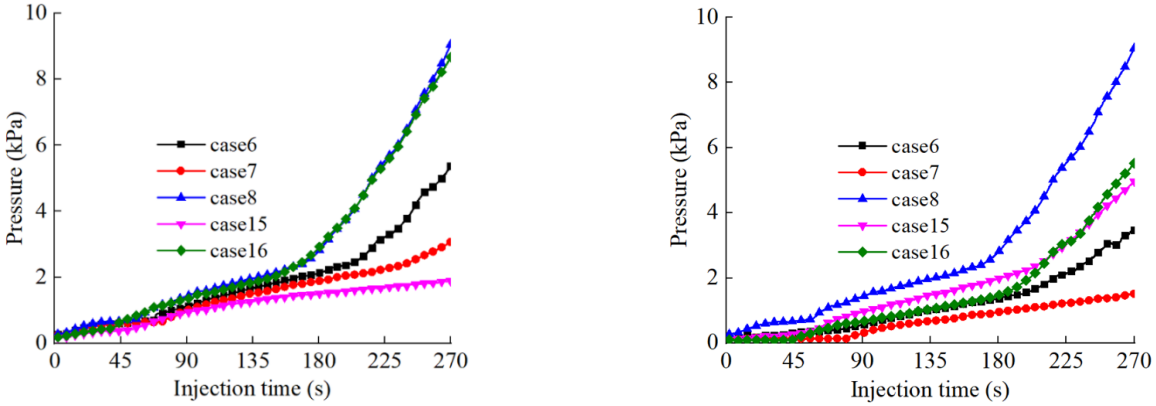

(a) Pressure under distal borehole (b) Pressure under proximal borehole

Fig. 6 Pressure variation under grouting boreholes with time

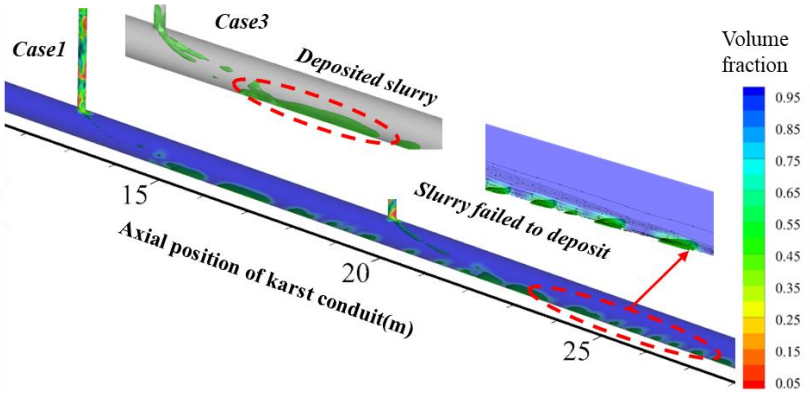

Fig. 7 Comparison of slurry diffusion between case1 and case3 at the initial stage of grouting

growth rate is obviously accelerated in this stage. According to the variations of flow rate and pressure in case6, the karst conduit was blocked at 240s, then the pressure increased rapidly, which doubled within 60 s. At this moment, the slurry is no longer occupying the position of water in the conduit, but squeezing previously deposited slurry. Therefore, the pressure continuously increases and pushes the slurry that has been deposited.

As shown in Fig. 6(b), in the initial stage, due to the pressure loss along the conduit, the pressure at the proximal borehole is lower than that at the distal borehole. With grouting going on, the pressure at the proximal borehole in case2 is higher than that at the distal borehole, while the pressure at the distal borehole in case7 is always higher than that at the proximal borehole. This phenomenon is caused by the difference of final blocking position. Due to the high grouting injection rate and strong time-dependent viscosity slurry used at the distal borehole in case7, the flowing water was blocked near the distal borehole. On the contrary, in case2 the flowing water was blocked at the proximal borehole. The proximal pressure increased faster and finally exceeded the distal pressure.

3.3.3 The behavior of flow and deposition in combined bi-borehole grouting

As shown in Fig. 7, at the beginning of grouting, case1 has low viscosity and high flow rate in the conduit, so the slurry cannot form stable deposition in the karst conduit. The slurry spreads downstream under the erosion of the water. The slurry has a tail of "pinnate" distribution, which migrates with the water to the outlet of the conduit. Part of the slurry finally flows out of the outlet. At this stage, the interaction of bi-borehole slurry is not obvious, which is similar to the single borehole grouting. On the contrary, when slurry of C:S=3:1 was used in case3, the slurry created a stable deposition area within 2-6m downstream of the proximal borehole, which avoided the abundant outflow.

As shown in Fig. 8, we summarized the time distribution of slurry outflow in four typical cases. It can be seen that more than 78% of the slurry outflow occurred in the first 40 s. Among them, the slurry outflow rate in case3 in the first 40 s is less than 1%. And as case4 has the highest outflow rate, the slurry outflow rate in case 4 is 3.9%. It is proved that the parameters selected in case3 have better performance in slurry retention. In the following section, we will discuss how to optimize the parameters to improve blocking efficiency. In numerical simulation, the effect of outflow slurry is no longer considered, the viscosity of the slurry remaining in the conduit increases gradually.

In order to study the velocity in the conduit, taking case1 as an example, the velocity data on the axis and the characteristic positions above and below the axis are selected for analysis. As shown in Fig. 9(a), the initial hydrodynamic velocity is maintained on the axis and above

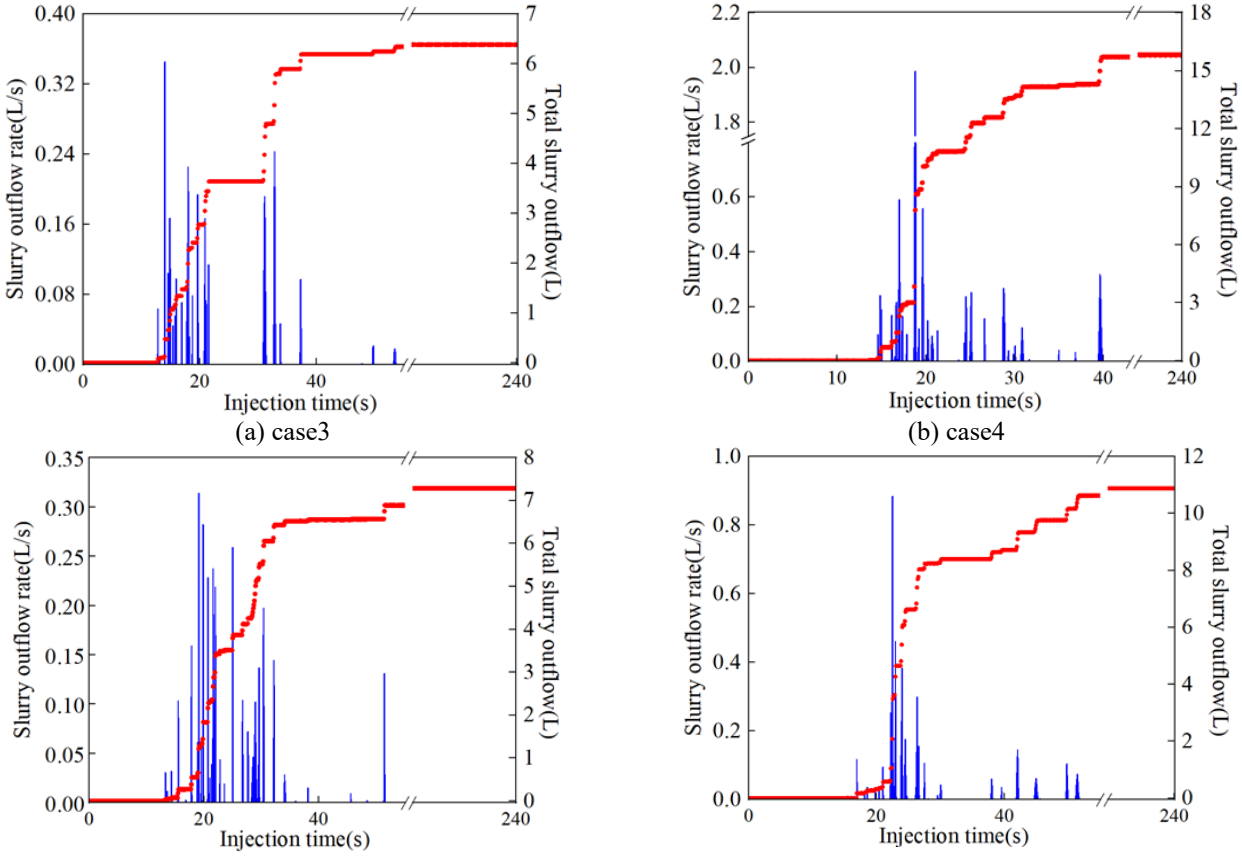

Fig. 8 Slurry outflow (blue strip) and accumulated outflow (red dot) of typical cases

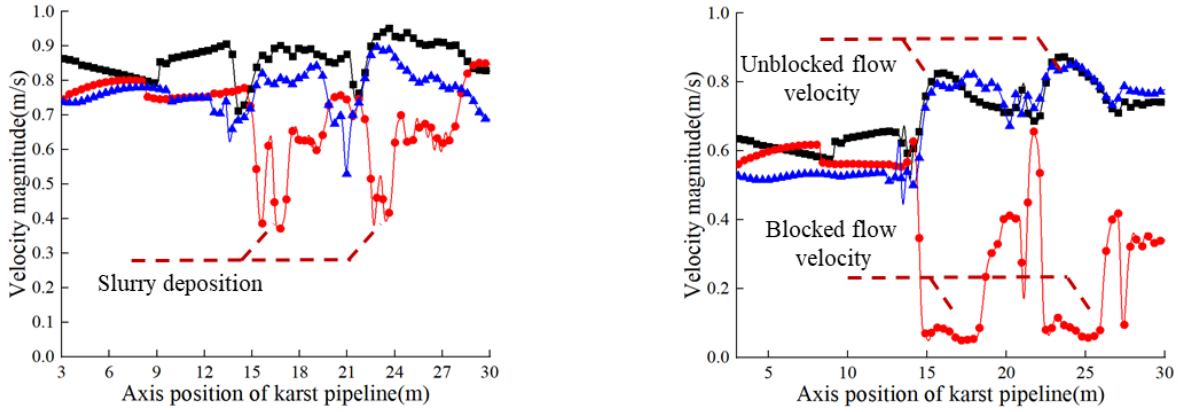

Fig. 9 Velocity variation of case 1 on the axis (black curves), above axis (blue curves) and below axis (red curves) of karst conduit

the axis in the first 20 s. The flow velocity of the slurry under the axis is obviously lower, but it is still greater than 0.4 m/s, which failed to block water. At 46 s, some of the slurry under the axis occured effective deposition, and the velocity was lower than 0.1 m/s, which was significantly lower than that in the unblocked area above the axis. The flowing water blocking has been realized in this area.

As shown in Fig. 10, taking case1 as an example, the slurry has flowed to the downstream for more than 15 m at 50 s. Case3 is different from case1 as its proximal slurry viscosity increases faster than the distal slurry. Therefore, case3 has better blocking effect on distal slurry without deposition, and accelerates the deposition of slurry near the proximal borehole.

As shown in Fig. 11, the grouting continues and the slurry begins to appear countercurrent flow, the slurry keeps approaching upstream. This phenomenon shows that the slurry in the conduit has a large viscosity, and under the large pressure, the slurry eventually deposited in the upstream area of the distal borehole. The appearance of

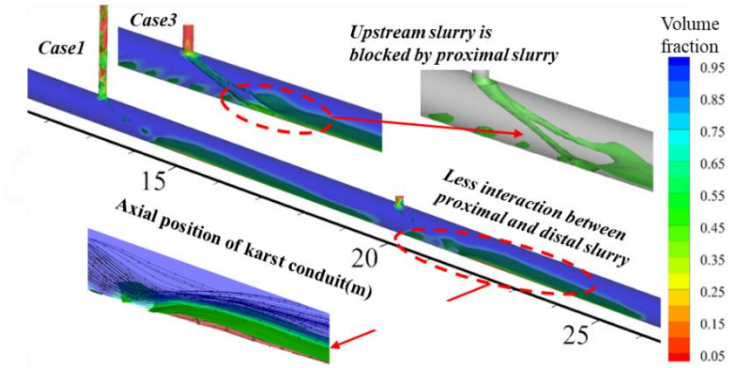

Fig. 10 Slurry deposition and water blocking effect of case1 and case3

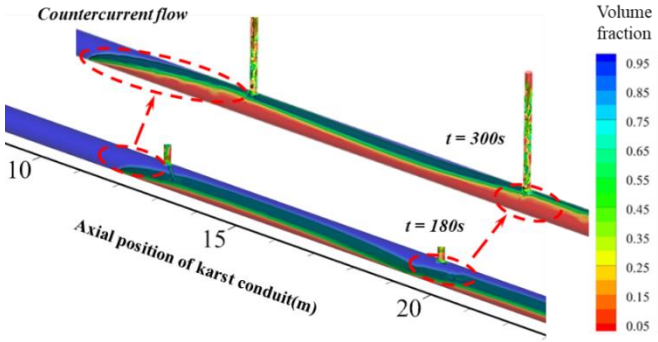

Fig. 11 Countercurrent diffusion and proximal borehole blocked in case1

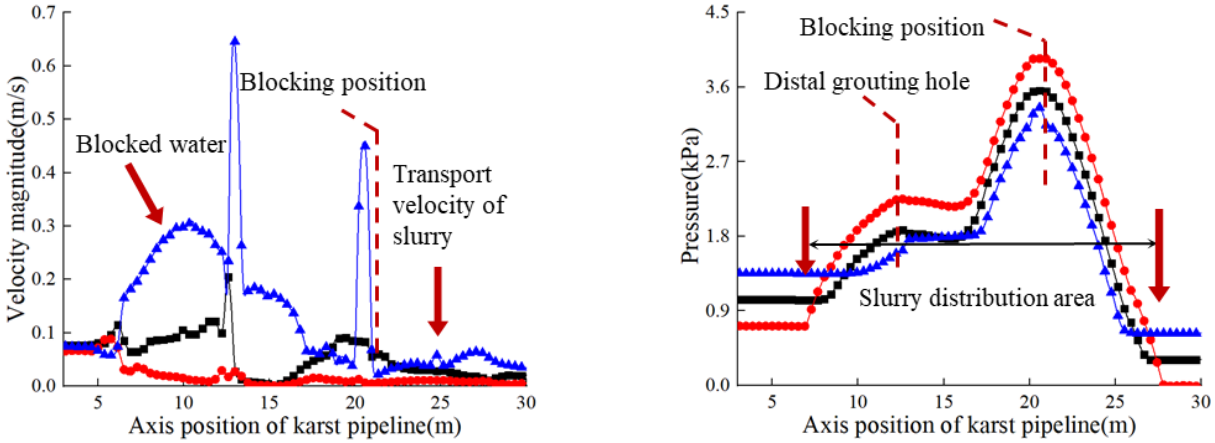

(a) Velocity distribution (b) Pressure distribution

Fig. 12 Velocity and pressure distribution of axis (black curves), above axis (blue curves) and below axis (red curves) in blocking completion stage of case3

counter current flow indicates that the velocity reduces and pressure rises in the conduit, which are the important criteria for blocking process in grouting. At this stage, the flow range of slurry has no obvious change, and the deposition thickness increases rapidly until a certain section is completely blocked.

The flow field situation of case3 is shown in Fig. 12. After the completion of blocking, the pressure decreases from the blocking position to both sides until it is beyond the scope of slurry deposition. The maximum pressure is more than 10 times greater than that in the initial stage of grouting. In terms of velocity distribution, the velocity along the axis and below the axis is close to zero. Due to the continuous slurry injection, there is slight flow above the axis. The flow in the upstream of the distal borehole is blocked to form a vortex, which has a large speed but cannot continue to move downstream.

3.4 Result analysis and optimization of orthogonal experiment

As shown in Fig. 13, through the single factor sensitivity analysis, the average value of time taken to achieve 90% flow reduction rate is compared with the five

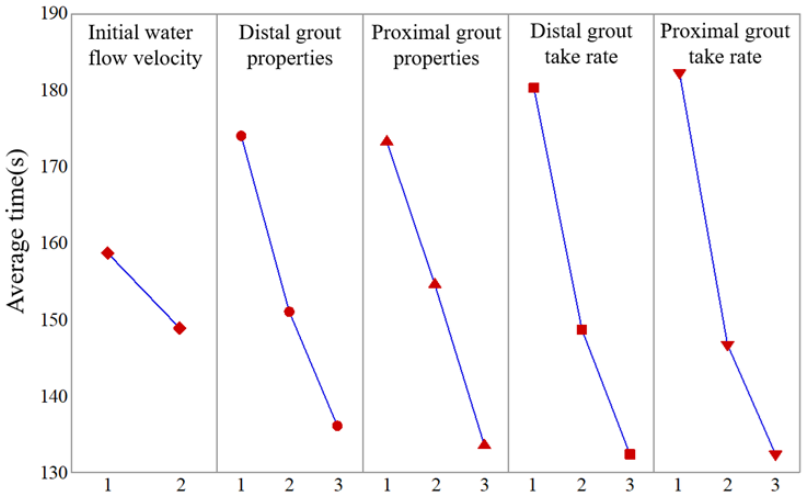

Fig. 13 Single factor sensitivity analysis

factors. It can be seen that the distal and proximal slurry injection rate has the greatest influence on blocking, and the blocking efficiency basically increases linearly with the increase of slurry injection rate. When the slurry injection rate of 0.2 m/s is selected, the average time of 90% blocking is more than 180 s, which is 38% longer than that when using the slurry injection rate of 0.5 m/s. Secondly, the properties of slurry also have great influence. With the use of strong viscosity time-dependent slurry, the blocking efficiency can be increased by 30% at most.

3.4.1 Influence analysis of slurry properties on blocking effect

Fig. 14 shows the effect on the average blocking time with different slurry properties at the proximal and distal boreholes. In general, the blocking efficiency can be improved by increasing the time-dependent behaviors of slurry viscosity. When both the proximal and distal boreholes adopt the slurry of C:S=1:1, the average time of blocking is more than 200 s. If the proximal borehole time-dependent behavior of slurry viscosity is changed separately, the blocking efficiency increases. By optimizing the matching of slurry properties, the average blocking time can be reduced by up to 40%. When the slurry of C:S=3:1 is selected for the distal borehole, the change of the slurry properties in the proximal borehole has no obvious influence on water blocking. When slurry of C:S=1:1 is selected at the distal borehole, different properties of slurry used in the proximal borehole will lead to great changes in the blocking efficiency. When the slurry of C:S=1:1 or 2:1 is used in the proximal borehole, the blocking process is relatively slow, with an average time of more than 190 s. However, when the slurry of C:S=3:1 is used in the proximal borehole, the average time to achieve blocking is reduced by more than 30%, which is the best among the various distal and proximal slurry collocations. If the properties of the proximal and distal grouting are reversed, the blocking time will be increased. When the slurry of C:S=2:1 is used at the distal and proximal boreholes, the effect of increasing the viscosity time-dependent behavior of slurry on accelerating the blocking is not obvious.

In case12, slurry of C:S=1:1 and 3:1 were used at the distal and proximal boreholes, respectively. The blocking time is 135 s, and the stable flow range of slurry is about 15.5 m. As to the shape of slurry deposition, case12 takes advantage of the strong time-dependent viscosity behavior of the proximal slurry to create a stable deposition area near the proximal borehole, and reduces the cross-sectional area of the karst conduit. The slurry with weak time-dependent behavior viscosity and good fluidity was injected at the distal borehole, and the slurry moved to the downstream with water flow. Under this condition, the upstream slurry is blocked by the high viscosity slurry which has been deposited near the proximal borehole, so it reduces slurry outflow. Meanwhile, the slurry viscosity increases continuously in the process of transportation. Finally, the distal and proximal slurry deposit near the proximal borehole together. Therefore, the selection of weak time-dependent viscosity behavior slurry in the distal borehole and strong time-dependent viscosity behavior slurry in the proximal borehole can significantly improve the blocking efficiency.

By contrast, in case11, due to the use of slurry with weak time-dependent viscosity behavior, its flow range is larger than that in case12, and there exists unstable deposition. This part of slurry finally flows out of the karst conduit and only keeps limited contribution.

3.4.2 Influence analysis of slurry injection rate on blocking effect

Fig. 15 shows the effect of different slurry injection rates at the proximal and distal boreholes on the blocking time. When the slurry injection rate is 0.5 m/s at the distal borehole, 0.35 ~ 0.5 m/s at the proximal borehole, or 0.5 m/s at the proximal borehole and 0.2m/s at the distal borehole, the average time of blocking is the fastest. When the slurry injection rate of 0.2m/s is used at both the distal and proximal boreholes, the blocking efficiency is significantly lower than those in other conditions, the blocking time will increase by over 75%. However, when the slurry injection rate of 0.2 m/s is not used simultaneously at the distal and proximal boreholes, the

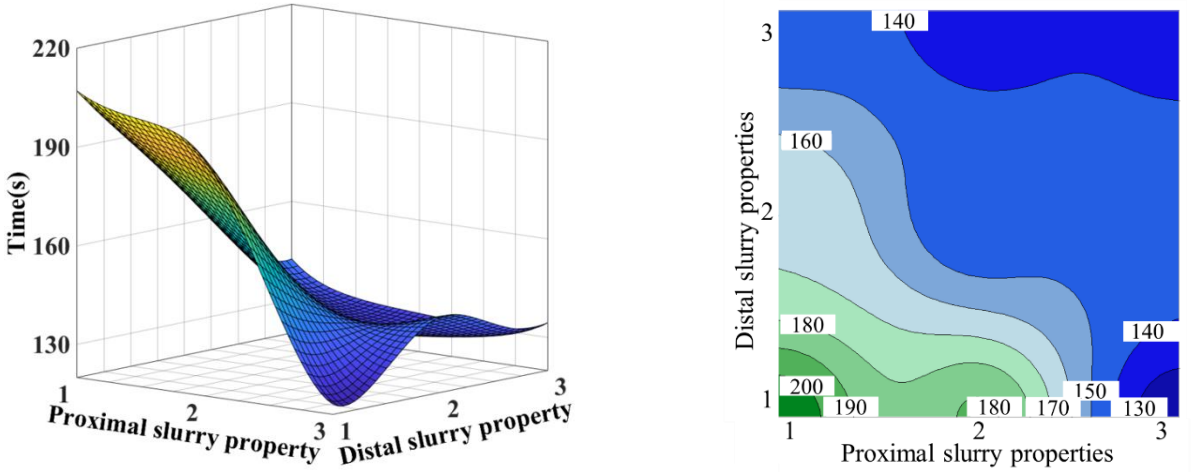

(a) Three dimensional response surface (b) Two dimensional contour

Fig. 14 Relationship between slurry properties and average blocking time

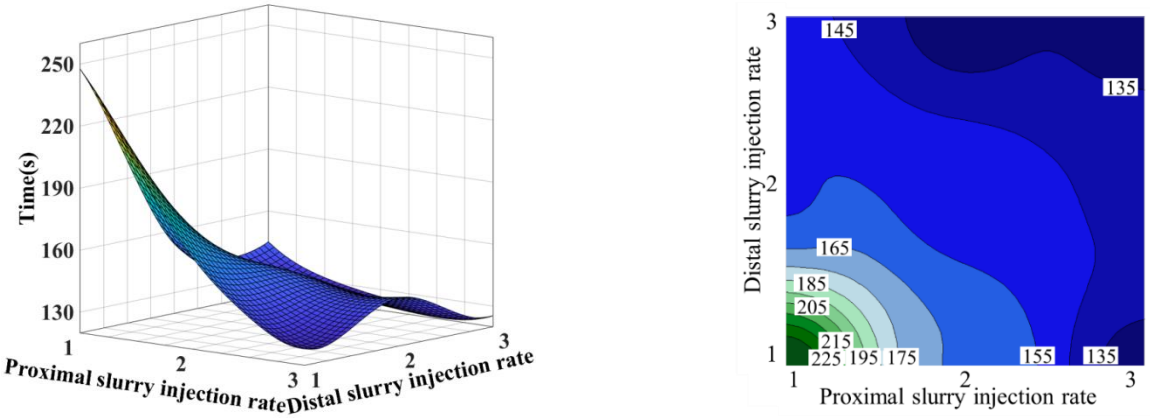

(a) Three dimensional response surface (b) Two dimensional contour

Fig. 15 Relationship between slurry injection rate and average blocking time

difference of blocking efficiency is relatively small, which is less than 23% compared with that in the fastest case. Among all the cases, case1 uses a slurry injection rate of 0.2 m/s for both boreholes. In a long time, the amount of slurry in the conduit is not enough to support the completion of blocking. For comparison, in case10, the slurry injection rate of 0.5 m/s is adopted for both boreholes. Although both cases adopt the slurry of C:S=1:1, the blocking time is reduced by more than 50%.

Through the above analysis, the scheme of "intercept the flow from the proximal borehole by quick-setting slurry and grout cement slurry from the distal borehole" was proposed. This scheme is conducive to the formation of a barrier near the proximal borehole and helps to avoid the outflow of upstream slurry. Meanwhile, it also enhances the blocking effect by making distal slurries deposit near the proximal borehole.

3.4.3 Influence of conduit geometry on blocking efficiency

Above analysis has revealed an efficient grouting scheme in combined bi-borehole grouting. However, it needs to be verified whether the variation of conduit geometry affects the scheme. For this purpose, the diameter of the conduit is replaced by 0.4 m and 0.6 m, respectively for numerical verification.

Table 3 Calculation parameters for different conduit geometries

Level	Conduit diameter (m)	Distal slurry properties (C:S)	Proximal slurry properties (C:S)	Slurry injection rate (m/s)
Case19	0.4	1:1	3:1	0.5
Case20		3:1	1:1	
Case21	0.6	1:1	3:1	
Case22		3:1	1:1	

Two groups of contrast cases were analyzed, as shown in Table 3. For the conduit with a diameter of 0.4 m, slurries of C:S=1:1 and C:S=3:1 are used in the distal and proximal borehole, respectively in case19. In case20, the slurry properties are reversed while maintaining the same initial flow velocity and slurry injection rate. For the conduit with a diameter of 0.6 m, same option is adopted. According to above conclusion, case19 and case21 should present better blocking efficiency.

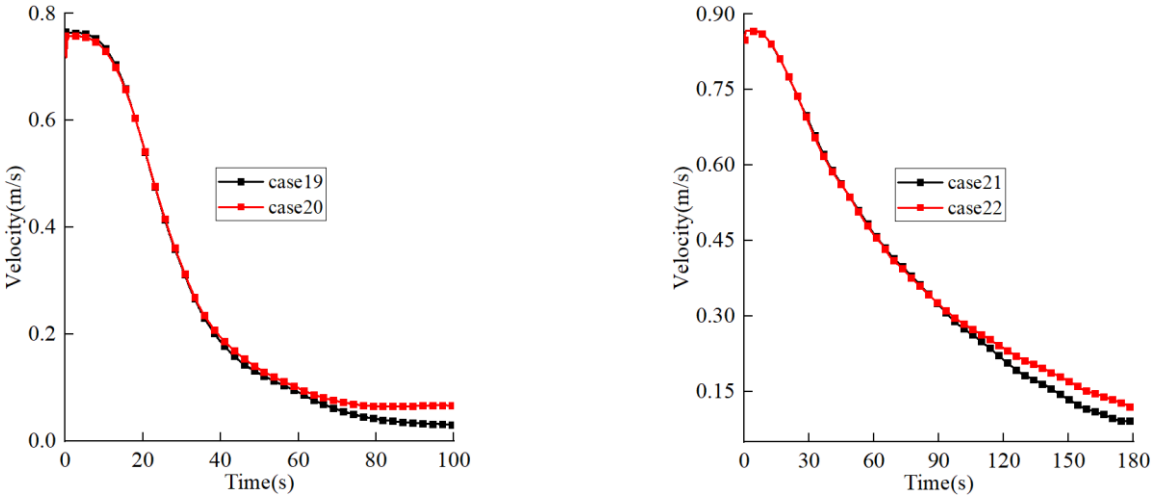

(a) Conduit diameter 0.4 m (b) Conduit diameter 0.6 m

Fig. 16 Contrast cases for the conduits with diameters of 0.4 m and 0.6 m

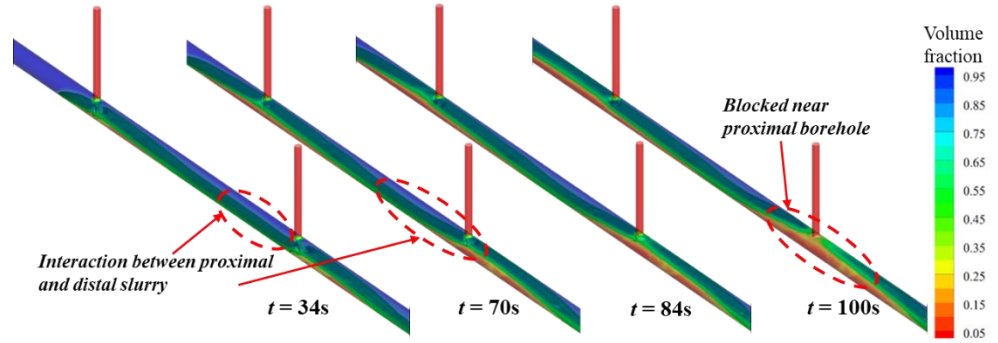

(a) Slurry diffusion in case19

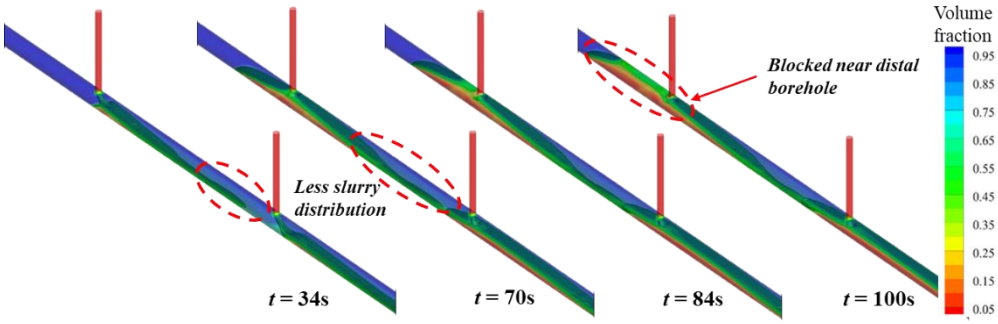

(b) Slurry diffusion in case20

Fig. 17 Slurry diffusion in case19 and case20.

As shown in Fig. 16, contrast cases perform similar velocity variation in the early stage of grouting since the distal and proximal slurry are separated from each other. For the conduit with a diameter of 0.4 m, the advantages of flow reduction in case19 is represented after 40 s. Similar phenomenon appears in the conduit with a diameter of 0.6 m, case21 showed better efficiency than case22 after about 90 s. As shown in Fig. 17, the primary difference betweencase19 and case20 is, the water is blocked near proximal borehole in case19 but it is blocked near the distal borehole in case20, instead. Thus, there is more efficient interaction between the distal and proximal slurries in case19. In this part, our previous conclusion is proved to be still valid in variable conduit geometries.

4. Engineering application

China Resources Cement (Pingnan) Limestone Mine is a water inflow treatment project located in Guangxi, China. The mining area is surrounded by water from three sides. As shown in Fig. 18, the east, north and south sides of the mining area are Qinchuan River, Nameless River and Xun River, respectively. The water level of Xun River ranges

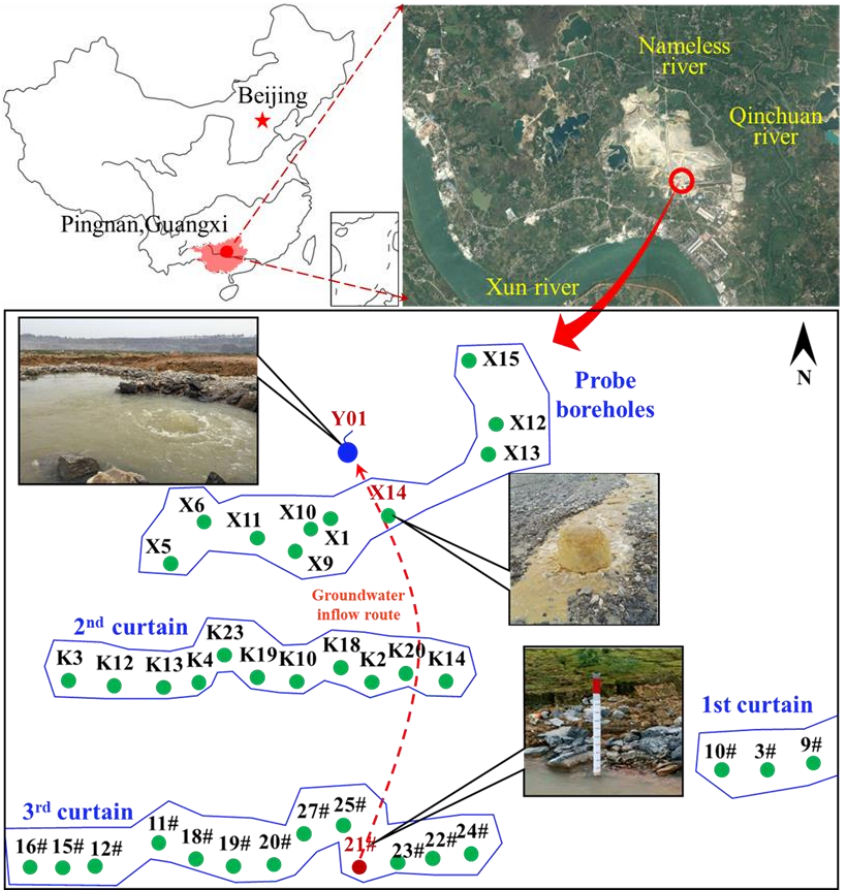

Fig. 18 Location and profile of China Resources Cement (Pingnan) Limestone Mine

(a) Before treatment (b) After treatment

Fig. 19 Comparison of the Y01 water inflow point before and after treatment (Li 2018)

from 34.03 m to 12.60 m above sea level. The abundant water of Xun River and Qinchuan river has become the main source of water inflow.

The mining method of open pit is adopted in this mine, and the mining depth is about 45 ~ 55 m. There are more than 10 water inflow points in the mine, which makes the daily water inflow more than 235 000 m^3. Among them, the elevation of water inflow point Y01 is -5 m and its daily water inflow is more than 71 200 m^3. A groundwater inflow funnel is formed in the mine. Surrounding groundwater discharges to the center of the funnel from the north-south and east-west karst channel. Based on previous prospecting, it is speculated that there are 4 karst groundwater runoffs in the east of the stope and 5 karst groundwater runoffs in the south.

The mining area is located in the east wing of Yujiang syncline, carbonate karst hydrogeological basin in Xunjiang Valley. The occurrence is about 156-174°,∠10-18°. Karst development decreases from the surface to the deep. At the elevation of 30 m to -10 m, the karst is relatively developed and there are many fractures and caves; at the elevation of -10 to -40 m, the karst development is reduced and karst development is weak below the elevation of -40 m. At the elevation of -5 m where the Y01 water inflow point is located, karst is well developed.

Considering the large space of mining area and high cost of continuous curtain, three discontinuous grout curtains were designed in this project, as shown in Fig. 18. The exploration of groundwater inflow route is the key to treatment since the limited blocking effect of discontinuous curtain and complex geological conditions. In geophysical prospecting, low resistivity was detected at about -50 m of the borehole 21# and -20 m, -40 m of the borehole X14, which is speculated as the main water inflow channel. The borehole 21# is at the upstream of the borehole X14 and both were confirmed as water inflow channels. This channel includes fracture and conduit water inflow. It is speculated that the category of water inflow is composed of conduits and fractures. Due to the wide range and huge water inflow of this limestone mine, the combined bi-borehole grouting technology in practice is conducive to increase the retention of slurry and accelerate water blocking.

In this project, cement slurry refers to ordinary Portland cement slurry. The density of cement slurry is about 1.3 ~1.7 g/cm³. Quick-setting slurry is the mixture of cement and sodium silicate, which is injected with a certain proportion. The volume ratio of cement to sodium silicate is generally between 1:1 and 3:1. The material properties are similar to the slurry used in numerical simulation, the time dependent viscosity functions are shown in Fig. 4. Meanwhile, the aggregates with poor fluidity is also used as filler materials in conduits and wide fractures. The solidification time of the quick-setting slurry is shorter and its diffusivity is weaker, it is not suitable for long distance transportation in karst conduits.

The specific implementation method of the combined bi-borehole grouting technology is: the aggregate and quick-setting slurry with strong time-dependent viscosity behavior is injected into the proximal borehole, and the cement slurry with weak time-dependent viscosity behavior and good fluidity is used in the distal borehole. In the proximal borehole, the quick-setting slurry can form stable deposition rapidly, and it is not easy to be affected by the flowing water while it is likley to form a blocking barrier in the downstream. At the same time, the cement slurry injected in the distal borehole has better fluidity, it diffuses downstream, but is blocked by the proximal slurry and remains in the vicinity of the proximal borehole. The final setting strength of cement slurry is larger, which can present better blocking effect. As shown in Fig. 19, through tracer experiment, it is verified that there is good connectivity between the borehole X14, borehole 21# and water inflow point Y01. Finally, the Y01 water inflow point and small water inflow points around were successfully blocked after the combined bi-borehole grouting treatment and subsequent consolidation. The total water reduction quantity is 843 00 m^3 per day.

5. Conclusions

Based on the sequential diffusion solidification (SDS) method considering the temporal and spatial evolution of the slurry viscosity, the mechanism of combined bi-borehole grouting technology for karst conduit was studied, the following conclusions are obtained:

In the initial stage of blocking, the slurry cannot be deposited effectively. The slurry outflow is concentrated in this stage. For most cases, the outflow rate is less than 5%. The basic mechanism of improving blocking efficiency by combined bi-borehole grouting is: the proximal slurry deposits at the bottom of the conduit to create a barrier, which prevents the slurry outflow from upstream and reduces the flow velocity in the conduit.

Through orthogonal experiment, the influences of proximal and distal slurry properties, the initial flow velocity of the conduit and the proximal and distal slurry injection rate on the blocking efficiency are compared. Under the orthogonal experiment conditions, the slurry injection rate has the greatest impact on blocking. The results of multi-factor sensitivity analysis showed that, keep the slurry injection rate constant, using slurry with weak time-dependent viscosity behavior in the distal borehole and slurry with strong time-dependent viscosity behavior in the proximal borehole can significantly improve the blocking efficiency.

Based on the above numerical simulation and orthogonal experiment results, the treatment scheme "intercept the flow from the proximal borehole by quick-setting slurry and grout cement slurry from the distal borehole " is put forward. The scheme has been successfully applied to the water inflow treatment project of China Resources Cement in Pingnan, Guangxi and reduced 84 300 m^3 water per day.

Data Availability Statement

All data, models, and code generated or used during the study appear in the submitted article.

Acknowledgments

We would like to acknowledge the financial support from the National Natural Science Foundation of China (Grant No.: 52022053 ; 52109129), and the China Postdoctoral Science Foundation (Grand No. s: BX2021172; 2021M691953).

References

Aflaki, E. and Moodi, F. (2017), "Laboratory tests for studying the performance of grouted micro-fine cement", *Comput. Concrete*, **20**(2), 145-154. http://doi.org/10.12989/cac.2017.20.2.145.

Amadei, B. and Savage, W.Z. (2001), "An analytical solution for transient flow of Bingham viscoplastic materials in rock fractures", *Int. J. Rock Mech. Min. Sci.*, **38**(2), 285–296. https://doi.org/10.1016/S1365-1609(00)00080-0.

Andjelkovic, V., Lazarevic, Z., Nedovic, V. and Stojanovic Z. (2013), "Application of the pressure grouting in the hydraulic tunnels", *Tunn. Undergr. Sp. Tech.* **37**, 165–179. https://doi.org/10.1016/j.tust.2012.08.012.

Ao, X., Wang, X., Zhu, X., Zhou, Z. and Zhang, X. (2017), "Grouting simulation and stability analysis of coal mine goaf

considering hydromechanical coupling", *J. Comput. Civil. Eng.*, **31**(3), http://doi.org/10.1061/(asce)cp.1943-5487.0000640.

Chi, Y., Sarica, C. and Daraboina, N. (2019), "Experimental investigation of two-phase gas-oil stratified flow wax deposition in pipeline", *Fuel*, **247**, 113-125. http://doi.org/10.1016/j.fuel.2019.03.032.

Draganović A. and Stille H. (2014), "Filtration of cement-based grouts measured using a long slot", *Tunn. Undergr. Sp. Tech.*, **43**, 101-112. https://doi.org/10.1016/j.tust.2014.04.010.

El Tani M. (2012), "Grouting Rock Fractures with Cement Grout", *Rock. Mech. and Rock. Eng.*, **45**(4), 547-561. http://doi.org/10.1007/s00603-012-0235-0.

Funehag, J. and Thörn, J. (2018), "Radial penetration of cementitious grout-Laboratory verification of grout spread in a fracture model", *Tunn. Undergr. Sp. Tech.*, **72**, 228-232. https://doi.org/10.1016/j.tust.2017.11.020

Ghafar, A.N., Mentesidis, A., Draganovic, A. and Larsson, S. (2016), "An experimental approach to the development of dynamic pressure to improve grout spread", *Rock. Mech. Rock. Eng.*, **49**(9), 3709-3721. http://doi.org/10.1007/s00603-016-1020-2.

Ghareh, S., Kazemian, S. and Shahin, M. (2020), "Assessment of compressibility behavior of organic soil improved by chemical grouting: An experimental and microstructural study", *Geomech. Eng.*, **21**(4), 337-348. http://doi.org/10.12989/gae.2020.21.4.337.

Gullu, H. (2017), "A novel approach to prediction of rheological characteristics of jet grout cement mixtures via genetic expression programming", *Neural Comput. Appl.*, **28**(1), 407–420. https://doi.org/10.1007/s00521-016-2360-2.

Gustafson, G., Claesson, J. and Fransson, A. (2013), "Steering parameters for rock grouting", *J. Appl. Math.*, **2013**(1), 1-9. https://doi.org/10.1155/2013/269594.

Hao, M., Wang, F., Li, X., Zhang, B. and Zhong, Y. (2018), "Numerical and Experimental Studies of Diffusion Law of Grouting with Expansible Polymer", *J. Mater. Civ. Eng.*, **30**(2), http://doi.org/10.1061/(asce)mt.1943-5533.0002130.

Huang, S., Pei, Q., Ding, X., Zhang, Y., Liu, D., He, J. and Bian, K. (2020), "Grouting diffusion mechanism in an oblique crack in rock masses considering temporal and spatial variation of viscosity of fast-curing grouts", *Geomech. Eng.*, **23**(2), 151-163. http://doi.org/10.12989/gae.2020.23.2.151

Ismail, A.S.I., Ismail, I., Zoveidavianpoor, M., Mohsin, R., Piroozian, A. and Misnan, M.S. (2015), "Experimental investigation of oil–water two-phase flow in horizontal pipes: Pressure losses, liquid holdup and flow patterns", *J. Petrol. Sci. Eng.*, **127**, 409-420. http://doi.org/10.1016/j.petrol.2015.01.038.

Kaushal, D.R., Thinglas, T., Tomita, Y., Kuchii, S. and Tsukamoto, H. (2012), "CFD modeling for pipeline flow of fine particles at high concentration", *Int. J. Multiphas. Fl.*, **43**, 85-100. http://doi.org/10.1016/j.ijmultiphaseflow.2012.03.005.

Kim, Y. and Moon, J. (2020), "Change of groundwater inflow by cutoff grouting thickness and permeability coefficient", *Geomech. Eng.*, **21**(2), 165-170. http://doi.org/10.12989/gae.2020.21.2.165

Lee, C.H., Low, Y.M. and Chiew Y.M. (2016), "Multi-dimensional rheology-based two-phase model for sediment transport and applications to sheet flow and pipeline scour", *Phys. Fluids*, **28**(5), http://doi.org/10.1063/1.4948987.

Li, H. (2018), "Study on Plugging Mechanism and Technology of Large-flow Karst Pipe Water Gushing", Ph.D. Dissertation; Shandong University, Jinan, China.

Li, S., Han, W., Zhang, Q., Liu, R. and Weng, X. (2013), "Research on Time-dependent Behavior of Viscosity of Fast Curing Grouts in Underground Construction Grouting", *Chinese J. Rock. Mech. Eng.*, **32**(1), 1-7. http://doi.org/10.1016/0006-8993(92)90961-8.

Li, S., Pan, D., Xu, Z., Lin, P. and Zhang, Y. (2020), "Numerical simulation of dynamic water grouting using quick-setting slurry in rock fracture: the Sequential Diffusion and Solidification (SDS) method", *Comput. Geotech.*, **122**, http://doi.org/10.1016/j.compgeo.2020.103497.

Liu, B., Sang, H., Liu, Q., Kang, Y., Pan, Y. and Lu, C. (2020), "New Algorithm for Simulating Grout Diffusion and Migration in Fractured Rock Masses", *Int. J. Geomech.*, **20**(3), http://doi.org/10.1061/(asce)gm.1943-5622.0001537.

Magnini, M. and Matar, O.K. (2019), "Fundamental study of wax deposition in crude oil flows in a pipeline via interface-resolved numerical simulations", *Ind. Eng. Chem. Res.*, **58**(47), 21797-21816. http://doi.org/10.1021/acs.iecr.9b05250.

Nadimi, S. and Shahriar, K. (2014), "Experimental creep tests and prediction of long-term creep behavior of grouting material", *Arabian J. Geosci.* **7**(8), 3251-3257. https://doi.org/10.1007/s12517-013-0920-7.

Minto, J.M., MacLachlan E., El Mountassir G. and Lunn R. J. (2016), "Rock fracture grouting with microbially induced carbonate precipitation", *Water. Resour. Res.*, **52**(11), 8827-8844. https://doi.org/10.1002/2016WR018884.

Mohajerani, S., Baghbanan, A., Bagherpour, R. and Hashemolhosseini, H. (2015), "Grout penetration in fractured rock mass using a new developed explicit algorithm", *Int. J. Rock. Mech. Min.*, **80**, 412-417. http://doi.org/10.1016/j.ijrmms.2015.06.013.

Mohammed, M.H., Pusch, R., Knutsson, S. and Hellstr, G. (2014), "Rheological properties of cement-based grouts determined by different techniques", *Engineering*, **6**, http://doi.org/10.4236/eng.2014.65026.

Mu, W., Li, L., Yang, T., Yu, G. and Han, Y. (2019), "Numerical investigation on a grouting mechanism with slurry-rock coupling and shear displacement in a single rough fracture", *B. Eng. Geo. Environ.*, **78**(8), 6159-6177. http://doi.org/10.1007/s10064-019-01535-w.

Puay, H.T. and Hosoda, T. (2016), "Mathematical modeling of the injection of grout into a horizontal slot", *Int. J. Geomech.* **16**(4), https://doi.org/10.1061/(ASCE)GM.1943-5622.0000566.

Rahman, M., Håkansson, U. and Wiklund, J. (2015), "In-line rheological measurements of cement grouts: Effects of water/cement ratio and hydration", *Tunn. Undergr. Sp. Tech.*, **45**, 34-42. http://doi.org/10.1016/j.tust.2014.09.003.

Sharpe, C.J. (1990), "Experimental effectiveness of rock fracture grouting", Ph.D. Dissertation; The University of Arizona, Tucson.

Stille, H., Gustafson, G. and Hassler, L. (2012), "Application of New Theories and Technology for Grouting of Dams and Foundations on Rock", *Geotech. Geol. Eng.*, **30**(3)**,** 603-624. http://doi.org/10.1007/s10706-012-9512-7.

Sui, W., Liu, J., Hu, W., Qi, J. and Zhan, K. (2015), "Experimental investigation on sealing efficiency of chemical grouting in rock fracture with flowing water", *Tunn. Undergr. Sp. Tech.*, **50**, 239-249. http://doi.org/10.1016/j.tust.2015.07.012.

Wang, Y.H., Yang, P., Li, Z.T., Wu, S.J. and Zhao, Z.X. (2020), "Experimental-numerical investigation on grout diffusion and washout in rough rock fractures under flowing water", *Comput. Geotech.*, **126**, http://doi.org/10.1016/j.compgeo.2020.103717.

Xu, Z., Shi, H., Lin, P. and Liu, T. (2021a), "Integrated lithology identification based on images and elemental data from rocks", *J. Petrol. Sci. Eng.*, **205**, 108853. https://doi.org/10.1016/j.petrol.2021.108853.

Xu, Z.H., Wang, W.Y., Lin, P., Nie, L.C., Wu, J. and Li, Z.M. (2021b), "Hard-rock TBM jamming subject to adverse geological conditions: Influencing factor, hazard mode and a case study of Gaoligongshan Tunnel", *Tunn. Undergr. Sp. Tech.*, **108**, 103683. https://doi.org/10.1016/j.tust.2020.103683.

Xu, Z., Lin, P., Xing, H., Pan, D. and Huang, X. (2021c), "Hydro-mechanical coupling response behaviors in tunnel subjected to a water-filled karst cave", *Rock Mech. Rock Eng.*, **54**(8), 3737-3756. https://doi.org/10.1007/s00603-021-02423-0.

Xu, Z., Pan, D., Lin, P., Zhang, Q., Li, H. and Zhang, Y. (2021d), "Numerical investigation of flow control technology for grouting and blocking of flowing water in karst conduits", *Int. J. Numer. Anal. Met.*, **45**(12), 1712-1738. https://doi.org/10.1002/nag.3221.

Xu, Z., Pan, D., Li, S., Zhang, Y., Bu, Z. and Liu, J. (2022), "A grouting simulation method for quick-setting slurry in karst conduit: The sequential flow and solidification method", *J. Rock Mech. Geotech.*, https://doi.org/10.1016/j.jrmge.2021.11.006.

Yang, P., Liu, Y., Gao, S. and Xue, S. (2020), "Experimental investigation on the diffusion of carbon fibre composite grouts in rough fractures with flowing water", *Tunn. Undergr. Sp. Tech.*, **95**, http://doi.org/10.1016/j.tust.2019.103146.

Zou, L., Håkansson, U. and Cvetkovic, V. (2018), "Two-phase cement grout propagation in homogeneous water-saturated rock fractures", *Int. J. Rock. Mech. Min.*, **106**, 243-249. http://doi.org/10.1016/j.ijrmms.2018.04.017.

Zou, L., Jing, L. and Cvetkovic, V. (2017), "Modeling of flow and mixing in 3D rough-walled rock fracture intersections", *Adv. Water. Resour.*, **107**, 1-9. http://doi.org/10.1016/j.advwatres.2017.06.003.

CC